PNAS RESEARCH ARTICLE | EARTH, ATMOSPHERIC, AND PLANETARY SCIENCES

Atmospheric forcing dominates winter Barents-Kara sea ice variability on interannual to decadal time scales

Zhongfang Liu[a,1], Camille Risi[b], Francis Codron[c], Zhimin Jian[a], Zhongwang Wei[d], Xiaogang He[e], Christopher J. Poulsen[f], Yue Wang[a], Dong Chen[g], Wentao Ma[h], Yanyan Cheng[i], and Gabriel J. Bowen[j]

Edited by Michael Mann, Pennsylvania State University, University Park, PA; received November 15, 2021; accepted June 28, 2022

The last two decades have seen a dramatic decline and strong year-to-year variability in Arctic winter sea ice, especially in the Barents-Kara Sea (BKS), changes that have been linked to extreme midlatitude weather and climate. It has been suggested that these changes in winter sea ice arise largely from a combined effect of oceanic and atmospheric processes, but the relative importance of these processes is not well established. Here, we explore the role of atmospheric circulation patterns on BKS winter sea ice variability and trends using observations and climate model simulations. We find that BKS winter sea ice variability is primarily driven by a strong anticyclonic anomaly over the region, which explains more than 50% of the interannual variability in BKS sea-ice concentration (SIC). Recent intensification of the anticyclonic anomaly has warmed and moistened the lower atmosphere in the BKS by poleward transport of moist-static energy and local processes, resulting in an increase in downwelling longwave radiation. Our results demonstrate that the observed BKS winter sea-ice variability is primarily driven by atmospheric, rather than oceanic, processes and suggest a persistent role of atmospheric forcing in future Arctic winter sea ice loss.

winter sea ice | atmospheric circulation | atmospheric thermodynamics | ocean heat transport | Barents-Kara Sea

Significance

The recent decline and variability in Arctic winter sea ice have been viewed as a combined response to oceanic and atmospheric processes. Disentangling the relative importance of these processes is challenging due to strong ocean-atmosphere coupling. Here, we demonstrate that Barents-Kara Sea (BKS) winter sea ice variability is primarily driven by atmospheric, rather than oceanic, processes. Increased transport of atmospheric heat and moisture into the BKS region increases downward longwave radiation, contributing to warming and sea ice decline. Our results reinforce the importance of atmospheric processes for Arctic winter sea ice variability and changes and have potential implications for climate and environment in the Arctic and beyond.

Variation in Arctic winter (December–February) sea ice has received far less scientific and public attention than summer sea ice, largely due to the fact that winter sea ice has weaker trends and variability (1). Over the last two decades, however, the Arctic has witnessed a dramatic decline in winter sea ice, particularly in the Barents-Kara Sea (BKS), a hotspot of Arctic warming (2, 3), where the rate has quadrupled relative to the preceding two decades (*SI Appendix*, Fig. S1*A*) and is highest in the Arctic (1) (Fig. 1*A*). The BKS decline is responsible for one-third of the pan-Arctic winter sea ice loss over the past four decades (*SI Appendix*, Fig. S1) and determines, to a large extent, Arctic winter sea-ice trends and variability. Superimposed on the secular trend is a strong year-to-year sea ice variability, which mainly occurs in the BKS (*SI Appendix*, Fig. S2), with the historical sea ice low set in the winter 2017 (Fig. 1). The winter sea ice variability impacts the Arctic climate (4, 5), communities, and ecosystems (6, 7), and potentially contributes to increased midlatitude extreme weather and climate [(3, 8–16) and references therein].

The recent rapid decline in BKS winter sea ice has been largely attributed to both oceanic (2, 17–21) and atmospheric (22–28) processes, but the relative importance of these processes is still a matter of debate (21, 26). Observational studies have argued for a leading role of the Atlantic Water (AW) (Fig. 1*A*) and suggest that AW warming enhances ocean heat transport (OHT) through the Barents Sea Opening (BSO) accelerating BKS sea ice decline (2, 18, 21). Such a mechanism appears to be supported by both geological records (29) and climate simulations (17–19) but is inconsistent with evidence for the recent slowdown of the Atlantic Meridional Overturning Circulation (AMOC) (20, 30, 31), which is responsible for most of the poleward OHT in the North Atlantic (32). Furthermore, the calculated OHT through the BSO accounts for a small fraction (38%, a largest explained variance when OHT leads SIC by 4 mo) of the observed BKS sea ice concentration (SIC) (Fig. 1*B* and *SI Appendix*, Fig. S3*A*). This impact is even weaker on interannual time scales (detrended data) at which OHT explains only 13% of the variance in the observed BKS SIC (*SI Appendix*, Fig. S4*A*).

In contrast, there is increasing evidence that BKS sea ice variability is highly linked to atmospheric processes, including atmospheric temperature (33, 34), poleward heat and moisture transport (25, 27, 33, 35), downward infrared radiation (26, 28), and positive lapse-rate feedback (25, 34), all of which are largely controlled by large-scale atmospheric circulation patterns. Observations show that BKS winter SIC is more strongly linked to an anticyclonic anomaly over the region (Fig. 1*C*), with a maximum

Author contributions: Z.L. designed research; Z.L. and C.R. performed research; C.R., F.C., and Z.W. contributed new reagents/analytic tools; Z.L., Z.J., X.H., Y.W., D.C., W.M., and Y.C. analyzed data; Z.L. wrote the paper with contributions from C.R., F.C., X.H., C.J.P., and G.J.B.

The authors declare no competing interest.

This article is a PNAS Direct Submission.

[1]To whom correspondence may be addressed. Email: liuzf406@gmail.com.

This article contains supporting information online at http://www.pnas.org/lookup/suppl/doi:10.1073/pnas.2120770119/-/DCSupplemental.

Published August 29, 2022.

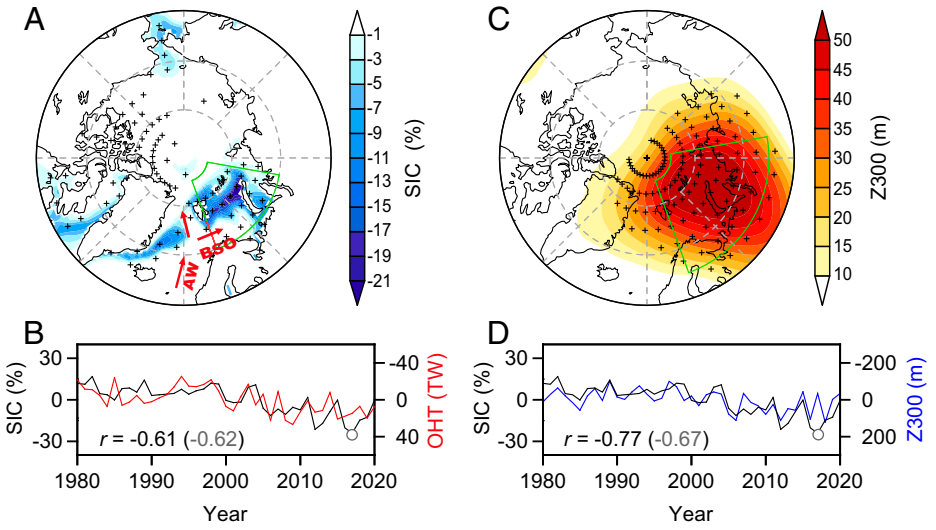

Fig. 1. Barents-Kara Sea (BKS) sea ice changes and its link to oceanic and atmospheric circulations over the period 1980–2020. (*A*) Linear trend (per decade) of winter (DJF) sea-ice concentration (SIC). (*B*) Time series of SIC anomaly averaged over the BKS with the strongest sea ice decline (20–80°E and 70–85°N; green box shown in *A*) and autumn (ASO) Atlantic Ocean heat transport (OHT) anomaly across the Barents Sea Opening (BSO; red line shown in *A*) (see *Materials and Methods*). (*C*) Winter 300-hPa geopotential height (Z300) regressed onto the standardized BKS SIC index defined in (*B*). (*D*) Time series of the BKS SIC and Z300 anomalies (area-averaged over the 20–100°E and 65–85°N; green box shown in *C*). The two seasons for oceanic and atmospheric circulation are chosen based on the maximum correlation between the circulation and SIC indices (*SI Appendix*, Fig. S3). Back and gray numbers in (*B*) and (*D*) show the correlations without and with winter 2017 (circle) included, respectively (*SI Appendix*, Text S1). Red arrows show the main pathways of Atlantic Water toward the Arctic in (*A*). The stippling in (*A*) and (*B*) indicates statistical significance at the 5% level.

correlation of −0.77 (Fig. 1*D* and *SI Appendix*, Fig. S3*B*) if winter 2016/17 (*SI Appendix*, Text S1 and Fig. S5), an outlier, is excluded (unless otherwise stated, the winter 2016/17 atmospheric circulation is not included in the following analysis). This link remains strong and robust ($r = -0.72$, $P < 0.01$) even after the long-term trends are removed (*SI Appendix*, Fig. S4*B*).

Disentangling the relative importance of oceanic and atmospheric processes in BKS winter sea ice variability is challenging, largely due to strong ocean-atmosphere coupling. In this study, we combine satellite observations of SIC (36), ERA5 atmospheric reanalysis (37), and numerical simulations (see *Materials and Methods*) to investigate the effect of atmospheric circulation patterns on BKS winter sea ice over the period 1980–2020 and the underlying physical mechanisms, demonstrating that atmospheric forcing, rather than oceanic forcing, is the dominant driver of Arctic winter sea ice variability.

Role of Atmospheric Circulation in Sea Ice Variability

During the study period, a winter anticyclonic anomaly, with an equivalent barotropic structure, strengthened over the BKS (*SI Appendix*, Fig. S6 *A* and *B*). This circulation pattern is neither obviously similar to the Arctic Oscillation (AO) (38) or the Arctic Dipole (AD) (39), nor does it follow summertime patterns that feature an anticyclonic anomaly over Greenland (GL-Z200) (40) or the western Arctic (41, 42). It is broadly similar to that associated with BKS winter SIC variability on both interannual (*SI Appendix*, Fig. S6 *C* and *D*) and decadal (Fig. 1*C*) time scales, supporting a robust link between BKS winter sea ice and atmospheric circulation patterns. Fig. 1*D* shows the temporal evolution of the indices of BKS SIC and anticyclonic anomalies. The BKS SIC, like the sea ice extent (*SI Appendix*, Fig. S1*A*), exhibits a significant negative trend (−6.5% per decade, $P < 0.01$) over the period 1980–2020, with strong interannual to decadal variability. Before 1999, the BKS SIC declined slowly with an insignificant trend of −0.7% per decade. Since then, the BKS SIC has declined at a faster rate (−8.1% per decade, $P < 0.01$ over the period 2000–2020) culminating in a record low in winter 2017. These changes in BKS SIC are mirrored by variations in the index of BKS anticyclonic anomaly, further corroborating the link between BKS sea ice and atmospheric circulation pattern.

To determine the cause-and-effect relationship between the identified BKS anticyclonic anomaly and SIC variability, we perform a lead-lag correlation analysis based on the indices of BKS SIC and anticyclonic anomalies. We find significant correlations when the BKS anticyclonic anomaly leads SIC by 0–4 mo, with a maximum for a zero lag (*SI Appendix*, Fig. S3*B*). In contrast, correlations are weak or insignificant when the BKS anticyclonic anomaly lags SIC by 1–2 mo. This suggests that atmospheric circulation is the driver of, not the response to, BKS sea ice variability (11). The BKS anticyclonic anomaly accounts for 59% of the variance in winter SIC over the study period, overshadowing the effect of OHT (Fig. 1 *B* vs. *D*). However, the influence of the BKS anticyclonic anomaly might be obscured by anthropogenic forcing. To circumvent this limitation, we examine the detrended data, hereafter referred to as "interannual." The BKS anticyclonic anomaly accounts for 52% of the interannual variance in SIC, comparable to the contribution (49%) of atmospheric internal variability estimated from the Coupled Model Intercomparison Project phase 6 (CMIP6) (43) preindustrial control (piControl) simulations (*SI Appendix*, Fig. S7). This indicates that winter sea ice variability in the BKS is largely dominated by the BKS anticyclonic anomaly, which far outweighs effects not only of anthropogenic forcing, but also of other large-scale oceanic or atmospheric circulation patterns reported previously (23, 24, 42, 44–46) (*SI Appendix*, Table S1). We therefore argue that the BKS anticyclonic circulation is the dominant driver of winter sea ice variability in the region, both on interannual and decadal time scales (*SI Appendix*, Fig. S8).

The cause and dominant role for atmospheric forcing on BKS winter sea ice variability is also supported by physical model simulations. We first run version 5A of the Laboratoire de Météorologie Dynamique-Zoom (LMDZ5A) (47) general

circulation model nudged toward reanalysis wind fields (labeled "forced-nudged simulation"), but with imposed climatological sea surface temperature (SST) and sea ice, as well as fixed CO_2 (see *Materials and Methods*). In a second simulation, we couple LMDZ5A to a slab ocean sea-ice model (labeled "slab-nudged simulation") with a flux correction to assess how SST and sea ice respond to the atmospheric forcing through thermodynamic processes (see *Materials and Methods*). Both simulations successfully reproduce the observed amplification of the anticyclonic circulation over the BKS (*SI Appendix*, Figs. S9 *A–C* and S10*A*). The anticyclonic anomaly leads to some significant model warming over the BKS, but the magnitude of these effects is systematically underestimated relative to observations (*SI Appendix*, Figs. S9 *D–F* and S10*B*). This underestimate is not unexpected considering the model limitations and our experiment design: the atmosphere–ice–ocean interactions are largely missing in the slab ocean-sea ice model, and anthropogenic warming was not included in our experiments. Simulated SIC mimics well the observed pattern and shows a declining trend in the Arctic, with the fastest rate in the BKS, but its magnitude is also underestimated (*SI Appendix*, Figs. S9 *G* and *H* and S10*C*). The underestimated trend in sea ice decline is largely because the model simulates lower SIC than observed before the mid-2000s (*SI Appendix*, Fig. S10*C*). This underestimate of winter ice growth is found in other sea ice models (48), but the reasons for it remain unclear. Despite these biases, our simulations accurately reproduce the interannual variability of Arctic winter climate and sea ice (*SI Appendix*, Fig. S10 *D–F*), which enables us to diagnose the role of atmospheric circulation in driving interannual variability of BKS sea ice and the associated physical mechanisms.

Fig. 2 compares the observed and simulated (slab-nudged simulation) Arctic SIC anomalies (Fig. 2 *A* and *B*) regressed onto the respective BKS anticyclonic indices, which show strong covariability with a shared variance of 97% (*SI Appendix*, Fig. S10*D*). The simulated Arctic SIC responses to interannual variability in the BKS anticyclonic anomaly bear a strong resemblance to the observed counterpart, with a pattern correlation of 0.82 over the entire Arctic north of 70°N. Both show the strongest sea ice decline in the BKS, where the simulated atmospheric forcing accounts for 64% of the observed interannual SIC variability (Fig. 2*D*). This atmospheric forcing is mainly manifested as the variability of the BKS anticyclonic anomaly, which explains 55% of the interannual SIC variance in our model (Fig. 2*E*), comparable to the observed target (52%) (Fig. 2*C*).

Role of Local Feedbacks in Sea Ice Variability

Although we have provided evidence that atmospheric forcing is the dominant driver of interannual variability in BKS sea ice, we have not ruled out the possible contribution of oceanic processes through feedbacks between sea ice and the atmosphere [sea ice loss can increase upward turbulent heat flux at the surface and therefore affect the atmospheric circulation (33, 49)]. To isolate the impact of atmospheric forcing from those caused by sea-ice feedbacks, we further compare the forced-nudged and slab-nudged simulations. Despite the substantial difference in SIC changes (the linear trend of SIC is close to zero in the forced-nudged simulation), both simulations exhibit very similar spatial patterns in tropospheric circulation and temperature trends, with enhanced anticyclonic anomaly and warming over the BKS (*SI Appendix*, Fig. S9 *B, C, E,* and *F*). These are comparable to the observed counterparts, but with a systematic underestimation of the warming trend (and thus sea ice decline) over the BKS (*SI Appendix*, Figs. S9 and S10 *A–C*). As stated above, this underestimate is associated with the model limitations and our experimental design. Regardless of these biases, the robust similarity in tropospheric circulation and low-level temperature trends between the two simulations suggests that the warming and sea ice decline in the BKS are largely a consequence of the atmospheric forcing. This inference is further confirmed by the thermodynamic responses to interannual variability of sea ice in the two modeling experiments. In the forced-nudged

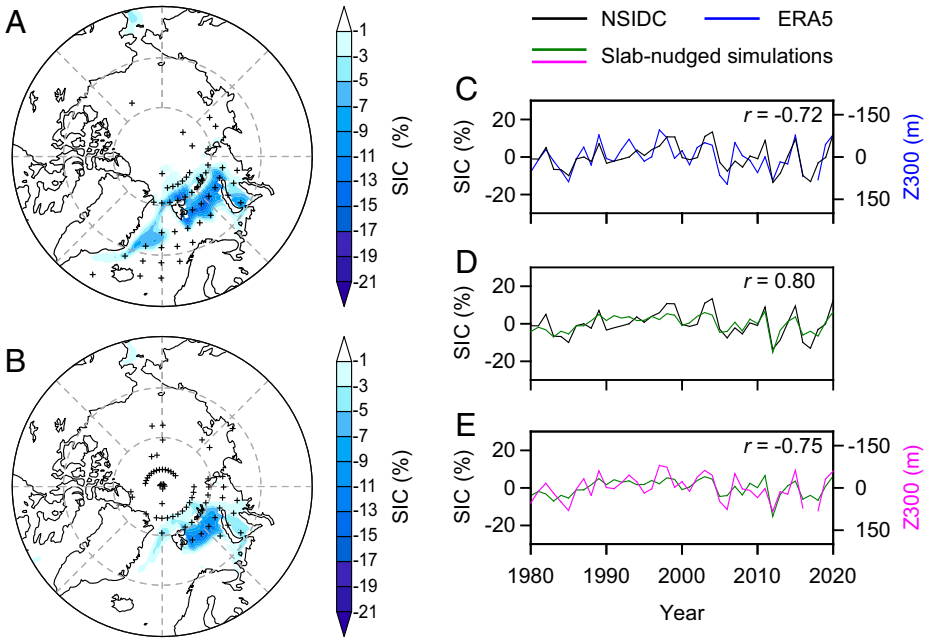

Fig. 2. BKS SIC responses to interannual variability in atmospheric circulation. (*A*) Detrended Arctic winter SIC anomalies regressed onto the standardized BKS circulation index (Z300) for observations. (*B*) Same as (*A*) but for the slab-nudged simulation. (*C*) Detrended time series of the BKS SIC and circulation anomalies for observations. (*D*) Detrended time series of the observed and simulated (slab-nudged) BKS SIC anomalies. (*E*) Same as (*C*) but for the slab-nudged simulation. Data of SIC and Z300 are obtained from the NSIDC and the ERA5, respectively. The stippling in (*A*) and (*B*) indicates statistical significance at the 5% level.

simulation, atmospheric forcing associated with the BKS anticyclonic anomaly results in significant lower-tropospheric warming and moistening, and thus increased surface downward longwave radiation (DLR) over the BKS, despite the absence of sea ice variability (*SI Appendix*, Fig. S11 *A*–*C*). Similar patterns are also seen in the slab-nudged simulation, but with slightly strengthened magnitude due to local feedbacks caused by sea ice reduction (*SI Appendix*, Fig. S11 *D*–*F*). Correlations indicate that these thermodynamic variables share approximately 90% of the variances between the forced-nudged and slab-nudged simulations (*SI Appendix*, Fig. S12), implying that local feedbacks may contribute about 10% to interannual variability of BKS temperature and sea ice. Our results are consistent with previous studies (11, 40) and corroborate that BKS winter sea ice variability is primarily driven by atmospheric forcing.

Thermodynamic Mechanisms for Atmospheric Forcing on Sea Ice Variability

To further understand the physical mechanisms at play, we investigate the thermodynamic processes associated with the BKS anticyclonic anomaly. Fig. 3 shows the thermodynamic responses to interannual variability in BKS anticyclonic anomaly in both reanalysis and slab-nudged simulation. The enhanced BKS anticyclonic anomaly is closely linked to increased transport of atmospheric heat and moisture from the Mediterranean–Black–Caspian seas and Baltic–North Sea regions (35) into the BKS, which raises temperature and humidity in the lower-troposphere and aloft (Fig. 3 and *SI Appendix*, Fig. S13) leading to increased DLR (25, 27, 35, 50) (Fig. 3 *C* and *F*). These conditions are probably enhanced by anticyclone-induced adiabatic subsidence (40), which amplifies bottom warming and causes a positive lapse-rate feedback [namely greater warming in the lower than upper troposphere (34)] (*SI Appendix*, Fig. S13 *A* and *C*), and by increased local moisture (12, 35), which warms and moistens the lower-level atmosphere by the upward infrared and turbulent fluxes (*SI Appendix*, Figs. S11 and S13). These combined thermodynamic processes melt or suppress the growth of sea ice in the BKS. The above diagnostic mechanisms are supported by strong interrelationships between the indices of BKS anticyclonic anomaly, thermodynamic parameters and SIC in both observations and slab-nudged simulation (*SI Appendix*, Fig. S14). Contrastingly over Eurasia, the atmospheric equatorward heat and moisture transport from the Arctic due to the BKS anticyclonic anomaly has caused cold and dry anomalies (Fig. 3). This contrasting pattern between the BKS and Asian continent is consistent with recent observational and modeling studies (10, 11), and has been attributed to tropical Pacific-driven poleward propagating waves (51–53) and Arctic atmospheric circulation rather than sea ice loss (11, 13, 54). Our work supports these studies and further reveals how the BKS anticyclonic anomaly drives sea ice variability through thermodynamic perturbations.

Cloud cover associated with the BKS anticyclonic anomaly may also contribute to Arctic winter sea ice variability through cloud-radiation feedback (33, 40, 50, 55). In winter during polar night, the downwelling shortwave radiation (DSR) can be neglected over the Arctic and cloud cover has a net greenhouse effect through creating strong DLR (49). Previous work indicates that increased low clouds due to an anticyclonic anomaly over Greenland contribute to Arctic summer sea ice loss (40). However, we find a strong decrease in winter low clouds over the BKS in reanalysis, which is not captured by our simulations, in response to enhanced anticyclonic anomaly (*SI Appendix*, Fig. S15 *A* and *D*). This is not unexpected given the anticyclone-driven adiabatic subsidence (56), which inhibits the formation of low clouds by warming and drying the lower-level atmosphere. By contrast, a slight increase in high clouds over the BKS is apparent in both reanalysis and simulations (*SI Appendix*, Fig. S15 *C* and *F*), largely a result of the intrusion of warm and moist air masses into the region (55, 57). This increase in high clouds that have a strong greenhouse effect (58, 59) may have partly contributed to BKS winter sea ice decline (60).

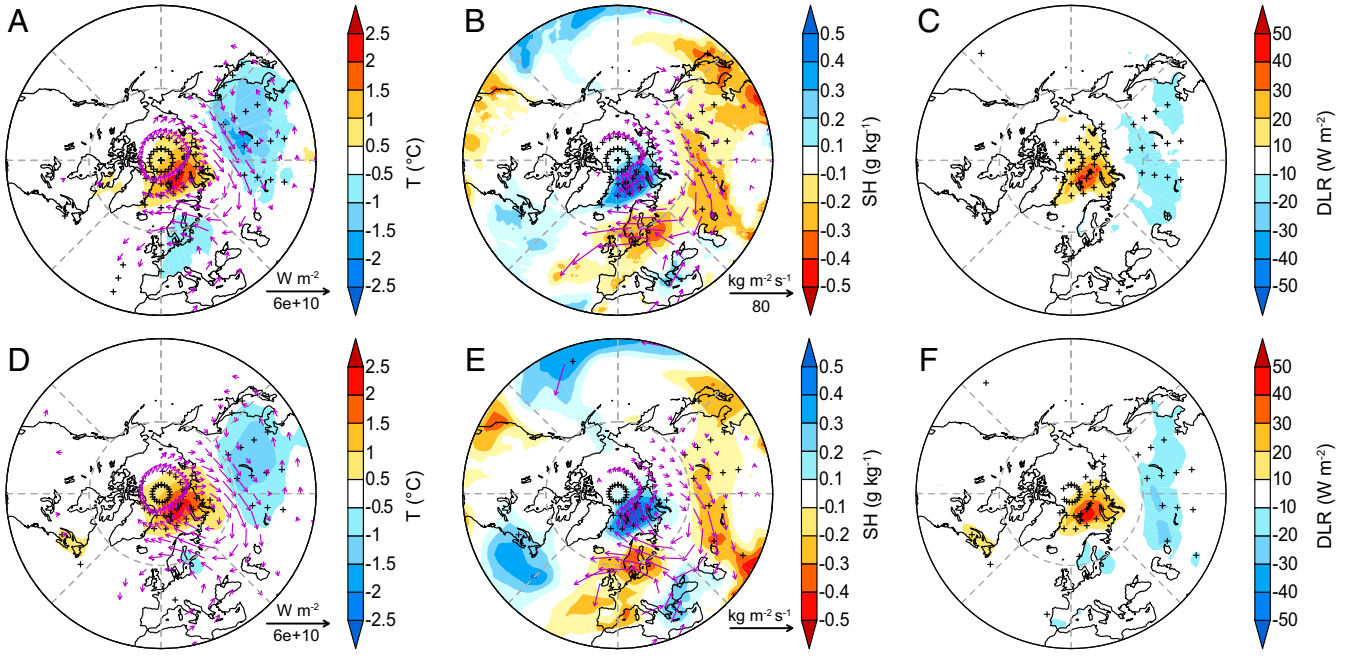

Fig. 3. Thermodynamic responses to interannual variability in BKS atmospheric circulation. (*A*) Regression patterns of the detrended winter lower-tropospheric (1,000–850 hPa) temperature (shading) and vertically integrated heat flux (arrows) onto the standardized BKS circulation index for observations. (*B* and *C*) Same as (*A*) but for lower-tropospheric (1,000–850 hPa) specific humidity (shading) and vertically integrated moisture flux (arrows; *B*), and downwelling longwave radiation (DLR) (*C*). (*D*–*F*) Same as (*A*)–(*C*) but for the slab-nudged simulation (Winter 2017 included). Shading with stippling indicates statistical significance at the 5% level in all plots. In (*A*), (*B*), (*D*), and (*E*), only vectors are shown when regressions are statistically significant at the 5% level.

Our simulations provide robust evidence that atmospheric forcing plays a more important role in driving BKS winter sea ice variability on interannual to decadal time scales than does oceanic forcing. This implies that atmospheric forcing is a dominant driver of ongoing Arctic winter sea-ice decline, given similar mechanisms at play. This atmospheric forcing mechanism itself is not new (25, 27, 33–35), but its dominance in Arctic winter sea ice variability over the past four decades has not been recognized, given the prevailing assumption that oceanic forcing plays a leading role in Arctic winter sea ice reduction (2, 18, 21). We cannot rule out the contribution or primacy of oceanic forcing to long-term (multidecadal or longer) Arctic sea variability because oceanic circulations have much longer time scales (61). In fact, some oceanic processes (e.g., AMOC) may have contributed to low-frequency variability in Arctic sea ice, accounting for the majority of the sea ice loss unexplained by atmospheric processes (45, 62). These oceanic processes reduce the thickness or formation of winter sea ice through warm AW transport and make BKS sea ice more susceptible to atmospheric forcing (63, 64).

Discussion and Summary

Despite the importance of an anticyclonic anomaly in driving Arctic winter sea ice variability, it is unclear whether it is a forced response or arises from internal variability. To address this, we turn to the latest-generation climate models from the CMIP6 (43). The CMIP6 multimodel ensemble mean (MMEM) for historical simulations appears to reproduce the observed anticyclonic circulation over the Arctic, but with a very weak anomaly and the center of action shifted substantially westward and northward (*SI Appendix*, Fig. S16*A*). This weak anticyclonic anomaly is generally associated with a reduction in Arctic SIC, especially in the BKS, where the strongest sea ice reduction in response to the BKS anticyclonic anomaly is well captured (Fig. 4 *A* and *B*). This adds further support that changes in BKS winter sea ice are closely linked to the BKS anticyclonic anomaly. The simulated BKS anticyclonic trend (44.9 m per 41 y, 1980–2020) in the MMEM, which removes internally generated variability and largely represents the externally forced response (10, 65), is much weaker than its observed counterpart (80.2 m per 41 y) and only accounts for 56% of the observed trend (Fig. 4 *C* and *D*). These differences in the location of the circulation center of action and trend probably reflect systematic biases in the CMIP models, which tend to underestimate the Arctic winter circulation anomaly and southerly moisture flux into the BKS (66, 67), and thus warming and sea ice reduction (68). On the other hand, these differences may imply that the observed BKS anticyclonic anomaly arises partly from internal variability superimposed on an externally forced response. The internally-induced BKS circulation trends (−13.5 m per 41 y for the MMEM) estimated from the piControl simulations, though exhibiting larger uncertainty, are generally less than those derived from the historical simulations (Fig. 4*C*). This can be interpreted to indicate that anthropogenic greenhouse forcing enhances the BKS circulation trend. Nonetheless, external forcing alone cannot explain the discrepancy between the observed and simulated BKS circulation trends. Thus, the observed, unusual BKS circulation trend might be partly due to internal variability. This inference is also confirmed by future high-emission scenario simulations (e.g., SSP5-8.5) that project an intensified anticyclonic anomaly over the Arctic, but with a pattern similar to neither observations nor historical simulations (*SI Appendix*, Fig. S16*B*).

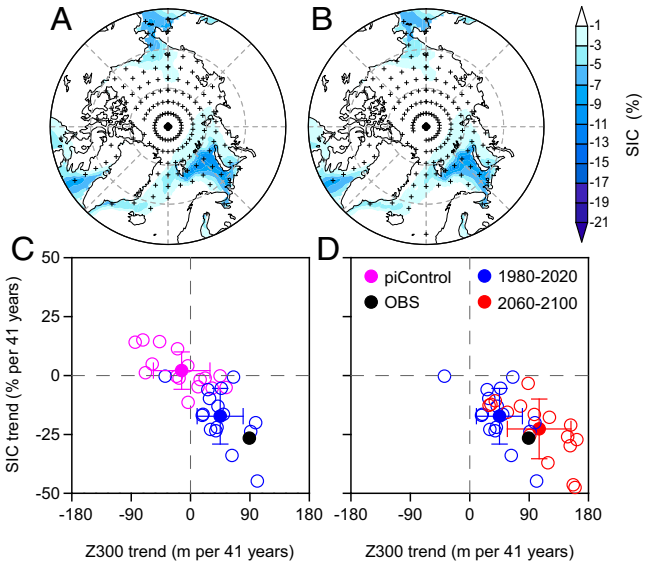

Fig. 4. CMIP6 multimodel simulated BKS SIC responses to atmospheric circulation changes. (*A*) Linear trend (per decade) of Arctic winter SIC in the multimodel ensemble mean (MMEM) over the period 1980–2020. (*B*) Arctic winter SIC regressed onto the standardized BKS circulation index in the MMEM. (*C*) Scatter plot of the BKS SIC and circulation trends from the historical and piControl simulations. (*D*) Same as (*C*) but for historical and ssp585 simulations. In (*C*), the trends in the piControl simulations are calculated based on 41-y-long nonoverlapping segments extracted from the simulations (see *Materials and Methods*). Open circles show the trends for individual models and solid circles for the MMEM (colored) with one SD (crosses) across models. Solid black circles in (*A*) and (*B*) denotes the observed trend (Winter 2017 included). The stippling in (*A*) and (*B*) indicates statistical significance at the 5% level.

Although the projected trend of the BKS anticyclonic index is more than doubled (105.1 m per 41 y, 2060–2100) during the latter decades of this century relative to the historical period (1980–2020), it is only close to the observed trend over the past decades. This suggests that a substantial part of the observed BKS circulation trend is due to internal variability (13) or that model projections underestimate the externally forced response. In sum, the observed BKS circulation trend discussed here is likely to arise from both internal variability and anthropogenic forcing, but the extent of the contribution from each is still an open question.

In conclusion, we demonstrate that Arctic winter sea ice variability and trends are primarily driven by a persistent anticyclonic anomaly over the BKS over the past decades. This circulation anomaly accounts for more than half of the year-to-year variability in BKS winter sea ice through a series of thermodynamic processes and is expected to further strengthen toward the end of this century under high-emission scenarios. Our results reconcile previous conflicting studies on the relative importance of oceanic and atmospheric processes (21, 26), as well as on the causal relationship between Arctic winter sea ice loss and atmospheric circulation (10, 11, 15). Given the simulated Eurasian cooling in response to the BKS anticyclonic anomaly, our work may also help clarify the cause of enhanced weather and climate extremes in northern midlatitudes, which largely arise from changes in BKS anticyclonic circulation rather than reduced sea ice (11, 13). Our study provides a perspective on the crucial role that large-scale atmospheric circulation plays in Arctic winter climate changes, which may have growing consequences for the trends, variability, and predictability of future Arctic sea ice and midlatitude weather extremes.

Materials and Methods

Model Simulations. The model simulations used here are taken from our recent work (42) that provides a detailed description of the models and experimental designs. A brief outline of model simulations is given here. We perform simulations with version 5A of the Laboratoire de Météorologie Dynamique-Zoom (LMDZ5A) (47) general circulation model, which is the atmospheric component of the Institute Pierre Simon Laplace (IPSL) coupled model IPSL-CM5A (69), coupled to a slab ocean sea-ice model (70). The model is run on a 1.875° × 3.75° (latitude × longitude) grid with 39 hybrid layers in the vertical dimension. The slab ocean is used as the surface model coupled to LMDZ5A, in which a simple thermodynamic sea-ice model (70) is included to provide an interactive representation of the sea ice. The heat transport by the ocean circulation is accounted for by adding a seasonally varying heat flux correction, usually referred to as Q-flux, to the surface heat fluxes. This heat flux is used to correctly reproduce the observed pattern of SST and sea ice.

We conduct two suites of model experiments. In the first experiment, the LMDZ5A is nudged toward the reanalyzed winds with a relaxation time of 1 h (71), but with imposed climatological sea surface temperature (SST) and sea ice conditions, as well as fixed CO_2. The simulation is run for 44 y (1977–2020), with the first 2 y considered as spin-up and thus discarded from the analysis (hereafter called "forced-nudged simulation"). In the second experiment, we include the same forcing, but couple the above LMDZ5A to the slab ocean sea-ice model with a heat flux correction (Q-flux) so that SST and sea ice can respond to the atmospheric forcing through thermodynamic processes (hereafter called "slab-nudged simulation"). The Q-flux is calculated for a monthly time scale based on the forced-nudged simulation described above, with conditions averaged over the period 1979–2020.

CMIP6 Simulations. To complement our analysis, monthly 300-hPa geopotential height (Z300) and sea ice concentration (SIC) outputs from 16 CMIP6 (43) models (accessed via the Earth System Grid Federation (ESGF) system at https://esgf-node.llnl.gov/search/cmip6) summarized in *SI Appendix*, Table S2 are used. All these models include the following standard experiments: preindustrial control (piControl), historical (1850–2014) and SSP5-8.5 (2015–2100) simulations. The historical and SSP5-8.5 simulations are forced with historical anthropogenic and natural forcings, and future high-emission scenario SSP5-8.5 (with a forcing of 8.5 W m^{-2} in 2100), respectively. The external forcings of the piControl simulation are held constant at preindustrial levels. As the length of the piControl simulation varies between models, we extract 42-y (41 winters) nonoverlapping samples from each model (to match the length of the observational record) for our analysis. Only the first realization (r1i1p1f1) is used here. To facilitate our analysis, all model data are interpolated onto a common 1° × 1° grid using a bilinear interpolation scheme.

Ocean Heat Transport. Ocean heat transport (OHT) across the Barents Sea Opening (BSO) (Fig. 1*A*) section is calculated as the spatial integral of the advective heat flux perpendicular to the grid cells from surface down to a depth of 300 m:

$$\mathrm{OHT} = \int_A c_p \rho_w U(T - T_{ref})\, dA$$

where c_p and ρ_w are the specific heat (3,850 J kg^{-1} K^{-1}) and density (1,025 kg m^{-3}) of seawater, U is the ocean velocity normal to the BSO section, A is surface area of the BSO section, T is the ocean potential temperature, and T_{ref} is the reference temperature that is set to 0 °C (18).

Observational and Reanalysis Data. The observed monthly sea ice concentration (SIC) (36) is provided by the National Snow and Ice Data Center (NSIDC) for the 1979–2020 (available at https://nsidc.org/data/nsidc-0116/versions/3). The atmospheric and oceanic data used here are taken from the ERA5 (37) and ORAS5 (72) reanalyses of the European Centre for Medium-Range Weather Forecasts (ECMWF), respectively (available at https://www.ecmwf.int/en/forecasts/datasets/reanalysis-datasets/era5 and https://www.ecmwf.int/en/research/climate-reanalysis/ocean-reanalysis, respectively). The ERA5 is the latest generation ECMWF atmospheric reanalysis, which includes several major technical improvements over its predecessor ERA-Interim (73) and a higher spatial and temporal resolution and thus has a better performance than its predecessor and others in the Arctic (74). The ORAS5 is an assimilated ocean reanalysis product developed using quality-controlled observations of SST, sea level anomaly, sea ice concentration as well as subsurface temperature and salinity profiles. It has been shown to provide realistic variability in ocean heat storage and oceanic transports in the Arctic (75), especially in the BKS (76).

Data, Materials, and Software Availability. Data (https://figshare.com/articles/dataset/Data_for_manuscript_Atmospheric_forcing_dominates_winter_Barents-Kara_sea_ice_variability_/20219036) (77) and code (https://figshare.com/articles/dataset/Codes_for_manuscript_Atmospheric_forcing_dominates_winter_Barents-Kara_sea_ice_variability_/20219189) (78) have been deposited in Figshare.

ACKNOWLEDGMENTS. This work was supported by the National Natural Science Foundation of China (42025602 and 41876039 to Z.L.). We thank the ECMWF for making the ERA5 and ORAS5 reanalysis datasets available for use. We acknowledge the World Climate Research Programme, which, through its Working Group on Coupled Modelling, coordinated and promoted CMIP6, and we thank the climate modeling groups (listed in *SI Appendix*, Table S2) for producing and making available their model outputs.

Author affiliations: [a]State Key Laboratory of Marine Geology, Tongji University, Shanghai 200092, China; [b]Laboratoire de Météorologie Dynamique, IPSL, CNRS, Sorbonne Université, Paris 75252, France; [c]Laboratoire d'Océanographie et du Climat, LOCEAN-IPSL, Sorbonne Université, CNRS, IRD, MNHN, Paris 75252, France; [d]Guangdong Province Key Laboratory for Climate Change and Natural Disaster Studies, School of Atmospheric Sciences, Sun Yat-sen University, Guangzhou 510275, China; [e]Department of Civil and Environmental Engineering, National University of Singapore, 117576, Singapore; [f]Department of Earth and Environmental Sciences, University of Michigan, Ann Arbor, MI 48109; [g]Nansen-Zhu International Research Centre, Institute of Atmospheric Physics, Chinese Academy of Sciences, Beijing 100029, China; [h]State Key Laboratory of Satellite Ocean Environment Dynamics, Second Institute of Oceanography, Ministry of Natural Resources, Hangzhou 310012, China; [i]Department of Industrial Systems Engineering and Management, National University of Singapore, 117576, Singapore; and [j]Department of Geology and Geophysics, University of Utah, Salt Lake City, UT 84112

1. I. H. Onarheim, T. Eldevik, L. H. Smedsrud, J. Stroeve, Seasonal and regional manifestation of Arctic sea ice loss. *J. Clim.* **31**, 4917–4932 (2018).
2. S. Lind, R. Ingvaldsen, T. Furevik, Arctic warming hotspot in the northern Barents Sea linked to declining sea-ice import. *Nat. Clim. Chang.* **8**, 634–639 (2018).
3. V. Petoukhov, V. A. Semenov, A link between reduced Barents-Kara sea ice and cold winter extremes over northern continents. *J. Geophys. Res.* **115**, 1–11 (2010).
4. L. Landrum, M. M. Holland, Extremes become routine in an emerging new Arctic. *Nat. Clim. Chang.* **10**, 1108–1115 (2020).
5. L. H. Smedsrud *et al.*, The role of the Barents Sea in the Arctic climate system. *Rev. Geophys.* **51**, 415–449 (2013).
6. E. Post *et al.*, Ecological consequences of sea-ice decline. *Science* **341**, 519–524 (2013).
7. M. Fossheim *et al.*, Recent warming leads to a rapid borealization of fish communities in the Arctic. *Nat. Clim. Chang.* **5**, 673–677 (2015).
8. J. Cohen *et al.*, Divergent consensuses on Arctic amplification influence on midlatitude severe winter weather. *Nat. Clim. Chang.* **10**, 20–29 (2020).
9. J. E. Overland *et al.*, Nonlinear response of mid-latitude weather to the changing Arctic. *Nat. Clim. Chang.* **6**, 992–999 (2016).
10. M. Mori, Y. Kosaka, M. Watanabe, H. Nakamura, M. J. N. C. C. Kimoto, A reconciled estimate of the influence of Arctic sea-ice loss on recent Eurasian cooling. *Nat. Clim. Chang.* **9**, 123–129 (2019).
11. R. Blackport, J. A. Screen, K. V. Der Wiel, R. Bintanja, Minimal influence of reduced Arctic sea ice on coincident cold winters in mid-latitudes. *Nat. Clim. Chang.* **9**, 697–704 (2019).
12. H. Bailey *et al.*, Arctic sea-ice loss fuels extreme European snowfall. *Nat. Geosci.* **14**, 283–288 (2021).
13. K. E. McCusker, J. C. Fyfe, M. Sigmond, Twenty-five winters of unexpected Eurasian cooling unlikely due to Arctic sea-ice loss. *Nat. Geosci.* **9**, 838–842 (2016).
14. R. Blackport, J. A. Screen, Observed statistical connections overestimate the causal effects of Arctic Sea ice changes on midlatitude winter climate. *J. Clim.* **34**, 3021–3038 (2021).
15. M. Mori, M. Watanabe, H. Shiogama, J. Inoue, M. Kimoto, Robust Arctic sea-ice influence on the frequent Eurasian cold winters in past decades. *Nat. Geosci.* **7**, 869–873 (2014).
16. R. Blackport, J. A. Screen, Weakened evidence for mid-latitude impacts of Arctic warming. *Nat. Clim. Chang.* **10**, 1065–1066 (2020).
17. Q. Wang *et al.*, Ocean heat transport into the Barents Sea: Distinct controls on the upward trend and interannual variability. *Geophys. Res. Lett.* **46**, 13180–13190 (2019).
18. M. Arthun, T. Eldevik, L. H. Smedsrud, O. Skagseth, R. Ingvaldsen, Quantifying the influence of Atlantic heat on Barents Sea ice variability and retreat. *J. Clim.* **25**, 4736–4743 (2012).
19. M. Arthun, T. Eldevik, L. H. Smedsrud, The role of Atlantic heat transport in future Arctic winter sea ice loss. *J. Clim.* **32**, 3327–3341 (2019).
20. T. Tsubouchi *et al.*, Increased ocean heat transport into the Nordic Seas and Arctic Ocean over the period 1993–2016. *Nat. Clim. Chang.* **11**, 21–26 (2021).
21. I. V. Polyakov *et al.*, Greater role for Atlantic inflows on sea-ice loss in the Eurasian Basin of the Arctic Ocean. *Science* **356**, 285–291 (2017).
22. A. Sorteberg, B. Kvingedal, Atmospheric forcing on the Barents Sea winter ice extent. *J. Clim.* **19**, 4772–4784 (2006).
23. J. Warner, J. Screen, A. Scaife, Links between Barents-Kara sea ice and the extratropical atmospheric circulation explained by internal variability and tropical forcing. *Geophys. Res. Lett.* **47**, e2019GL085679 (2020).

24. B. M. Hegyi, P. C. Taylor, The regional influence of the Arctic Oscillation and Arctic Dipole on the wintertime Arctic surface radiation budget and sea ice growth. *Geophys. Res. Lett.* **44**, 4341–4350 (2017).
25. C. Woods, R. Caballero, The role of moist intrusions in winter Arctic warming and sea ice decline. *J. Clim.* **29**, 4473–4485 (2016).
26. D. R. Park, S. Lee, S. B. Feldstein, Attribution of the recent winter sea ice decline over the Atlantic sector of the Arctic Ocean. *J. Clim.* **28**, 4027–4033 (2015).
27. H. Park, S. Lee, S. Son, S. B. Feldstein, Y. Kosaka, The impact of poleward moisture and sensible heat flux on Arctic winter sea ice variability. *J. Clim.* **28**, 5030–5040 (2015).
28. T. Gong, S. B. Feldstein, S. Lee, The role of downward infrared radiation in the recent arctic winter warming trend. *J. Clim.* **30**, 4937–4949 (2017).
29. R. F. Spielhagen *et al.*, Enhanced modern heat transfer to the Arctic by warm Atlantic Water. *Science* **331**, 450–453 (2011).
30. F. Sévellec, A. V. Fedorov, W. Liu, Arctic sea-ice decline weakens the Atlantic meridional overturning circulation. *Nat. Clim. Chang.* **7**, 604–610 (2017).
31. M. A. Srokosz, H. L. Bryden, OCEAN CIRCULATION. Observing the Atlantic Meridional Overturning Circulation yields a decade of inevitable surprises. *Science* **348**, 1255575 (2015).
32. M. W. Buckley, J. Marshall, Observations, inferences, and mechanisms of the Atlantic Meridional Overturning Circulation: A review. *Rev. Geophys.* **54**, 5–63 (2016).
33. D. Olonscheck, T. Mauritsen, D. Notz, Arctic sea-ice variability is primarily driven by atmospheric temperature fluctuations. *Nat. Geosci.* **12**, 430 (2019).
34. F. Pithan, T. Mauritsen, Arctic amplification dominated by temperature feedbacks in contemporary climate models. *Nat. Geosci.* **7**, 181–184 (2014).
35. L. Zhong, L. Hua, D. Luo, Local and external moisture sources for the Arctic warming over the Barents-Kara Seas. *J. Clim.* **31**, 1963–1982 (2017).
36. W. Meier *et al.*, *NOAA/NSIDC Climate Data Record of Passive Microwave Sea Ice Concentration, Version 3* (National Snow and Ice Data Center, NSIDC, 2020).
37. H. Hersbach *et al.*, The ERA5 global reanalysis. *Q. J. R. Meteorol. Soc.* **146**, 1999–2049 (2020).
38. D. W. Thompson, J. M. Wallace, The Arctic Oscillation signature in the wintertime geopotential height and temperature fields. *Geophys. Res. Lett.* **25**, 1297–1300 (1998).
39. B. Wu, J. Wang, J. E. Walsh, Dipole anomaly in the winter Arctic atmosphere and its association with sea ice motion. *J. Clim.* **19**, 210–225 (2006).
40. Q. Ding *et al.*, Influence of high-latitude atmospheric circulation changes on summertime Arctic sea ice. *Nat. Clim. Chang.* **7**, 289–295 (2017).
41. M. L. L'Heureux, A. Kumar, G. D. Bell, M. S. Halpert, R. W. Higgins, Role of the Pacific-North American (PNA) pattern in the 2007 Arctic sea ice decline. *Geophys. Res. Lett.* **35**, L20701 (2008).
42. Z. Liu *et al.*, Acceleration of western Arctic sea ice loss linked to the Pacific North American pattern. *Nat. Commun.* **12**, 1519 (2021).
43. V. Eyring *et al.*, Overview of the Coupled Model Intercomparison Project Phase 6 (CMIP6) experimental design and organization. *Geosci. Model Dev.* **9**, 1937–1958 (2016).
44. C. Deser, H. Teng, Evolution of Arctic sea ice concentration trends and the role of atmospheric circulation forcing, 1979–2007. *Geophys. Res. Lett.* **35**, L02504 (2008).
45. M. W. Miles *et al.*, A signal of persistent Atlantic multidecadal variability in Arctic sea ice. *Geophys. Res. Lett.* **41**, 463–469 (2014).
46. F. S. Castruccio *et al.*, Modulation of Arctic sea ice loss by atmospheric teleconnections from Atlantic multidecadal variability. *J. Clim.* **32**, 1419–1441 (2019).
47. F. Hourdin *et al.*, The LMDZ4 general circulation model: Climate performance and sensitivity to parametrized physics with emphasis on tropical convection. *Clim. Dyn.* **27**, 787–813 (2006).
48. D. Schröder, D. L. Feltham, M. Tsamados, A. Ridout, R. Tilling, New insight from CryoSat-2 sea ice thickness for sea ice modelling. *Cryosphere* **13**, 125–139 (2019).
49. J. A. Screen, I. Simmonds, The central role of diminishing sea ice in recent Arctic temperature amplification. *Nature* **464**, 1334–1337 (2010).
50. M.-L. Kapsch, R. G. Graversen, M. Tjernström, Springtime atmospheric energy transport and the control of Arctic summer sea-ice extent. *Nat. Clim. Chang.* **3**, 744–748 (2013).
51. S. Lee, Testing of the tropically excited Arctic warming mechanism (TEAM) with traditional El Niño and La Niña. *J. Clim.* **25**, 4015–4022 (2012).
52. J. P. Clark, S. Lee, The role of the tropically excited Arctic warming mechanism on the warm Arctic cold continent surface air temperature trend pattern. *Geophys. Res. Lett.* **46**, 8490–8499 (2019).
53. M. Park, S. Lee, The role of planetary-scale eddies on the recent isentropic slope trend during boreal winter. *J. Atmos. Sci.* **78**, 2879–2894 (2021).
54. J. A. Screen, R. Blackport, Is sea-ice-driven Eurasian cooling too weak in models? *Nat. Clim. Chang.* **9**, 934–936 (2019).
55. R. G. Graversen, T. Mauritsen, M. Tjernström, E. Källén, G. Svensson, Vertical structure of recent Arctic warming. *Nature* **451**, 53–56 (2008).
56. H. Wernli, L. Papritz, Role of polar anticyclones and mid-latitude cyclones for Arctic summertime sea-ice melting. *Nat. Geosci.* **11**, 108–113 (2018).
57. T. Nygård, R. G. Graversen, P. Uotila, T. Naakka, T. Vihma, Strong dependence of wintertime Arctic moisture and cloud distributions on atmospheric large-scale circulation. *J. Clim.* **32**, 8771–8790 (2019).
58. M. D. Zelinka, D. A. Randall, M. J. Webb, S. A. Klein, Clearing clouds of uncertainty. *Nat. Clim. Chang.* **7**, 674–678 (2017).
59. J. R. Norris *et al.*, Evidence for climate change in the satellite cloud record. *Nature* **536**, 72–75 (2016).
60. J. A. Beesley, Estimating the effect of clouds on the arctic surface energy budget. *J. Geophys. Res.* **105**, 10103–10117 (2000).
61. S. K. Gulev, M. Latif, N. Keenlyside, W. Park, K. P. Koltermann, North Atlantic Ocean control on surface heat flux on multidecadal timescales. *Nature* **499**, 464–467 (2013).
62. R. Zhang, Mechanisms for low-frequency variability of summer Arctic sea ice extent. *Proc. Natl. Acad. Sci. U.S.A.* **112**, 4570–4575 (2015).
63. M. A. Granskog *et al.*, Arctic research on thin ice: Consequences of Arctic sea ice loss. *Eos (Wash. D.C.)* **97**, 22–26 (2016).
64. T. Vihma, Effects of Arctic sea ice decline on weather and climate: A review. *Surv. Geophys.* **35**, 1175–1214 (2014).
65. D. Li, R. Zhang, T. R. Knutson, On the discrepancy between observed and CMIP5 multi-model simulated Barents Sea winter sea ice decline. *Nat. Commun.* **8**, 14991 (2017).
66. C. Woods, R. Caballero, G. Svensson, Representation of Arctic moist intrusions in CMIP5 models and implications for winter climate biases. *J. Clim.* **30**, 4083–4102 (2017).
67. S. Lee, C. Woods, R. Caballero, Relation between Arctic moisture flux and tropical temperature biases in CMIP5 simulations and its fingerprint in RCP8. 5 projections. *Geophys. Res. Lett.* **46**, 1088–1096 (2019).
68. R. Davy, S. Outten, The Arctic surface climate in CMIP6: Status and developments since CMIP5. *J. Clim.* **33**, 8047–8068 (2020).
69. J.-L. Dufresne *et al.*, Climate change projections using the IPSL-CM5 Earth System Model: From CMIP3 to CMIP5. *Clim. Dyn.* **40**, 2123–2165 (2013).
70. F. Codron, Ekman heat transport for slab oceans. *Clim. Dyn.* **38**, 379–389 (2012).
71. C. Risi, S. Bony, F. Vimeux, J. Jouzel, Water-stable isotopes in the LMDZ4 general circulation model: Model evaluation for present-day and past climates and applications to climatic interpretations of tropical isotopic records. *J. Geophys. Res.* **115**, 1–27 (2010).
72. H. Zuo, M. A. Balmaseda, S. Tietsche, K. Mogensen, M. Mayer, The ECMWF operational ensemble reanalysis–analysis system for ocean and sea ice: A description of the system and assessment. *Ocean Sci.* **15**, 779–808 (2019).
73. D. Dee *et al.*, The ERA-Interim reanalysis: Configuration and performance of the data assimilation system. *Q. J. R. Meteorol. Soc.* **137**, 553–597 (2011).
74. R. M. Graham *et al.*, Evaluation of six atmospheric reanalyses over Arctic sea ice from winter to early summer. *J. Clim.* **32**, 4121–4143 (2019).
75. P. Uotila *et al.*, An assessment of ten ocean reanalyses in the polar regions. *Clim. Dyn.* **52**, 1613–1650 (2019).
76. Q. Shu, Q. Wang, Z. Song, F. Qiao, The poleward enhanced Arctic Ocean cooling machine in a warming climate. *Nat. Commun.* **12**, 2966 (2021).
77. Z. Liu, Atmospheric forcing dominates winter Barents-Kara sea ice variability. Figshare. https://figshare.com/articles/dataset/Data_for_manuscript_Atmospheric_forcing_dominates_winter_Barents-Kara_sea_ice_variability_/20219036. Deposited 3 July 2022.
78. Z. Liu, Atmospheric forcing dominates winter Barents-Kara sea ice variability. Figshare. https://figshare.com/articles/dataset/Codes_for_manuscript_Atmospheric_forcing_dominates_winter_Barents-Kara_sea_ice_variability_/20219189. Deposited 3 July 2022.